PHOTOCOLOURATION OF 2,4,4,6-TETRAARYL-4*H*-PYRANS AND THEIR HETEROANALOGUES: IMPORTANCE OF HYPERVALENT PHOTOISOMERS

Stanislav BOHM[a], Mojmir ADAMEC[b], Stanislav NESPUREK[b] and Josef KUTHAN[a]

[a] *Department of Organic Chemistry, Prague Institute of Chemical Technology, 166 28 Prague 6, Czech Republic*
[b] *Institute of Macromolecular Chemistry, Academy of Sciences of the Czech Republic, 162 06 Prague 6, Czech Republic*

Received May 12, 1995
Accepted June 19, 1995

Dedicated to Dr Blahoslav Sedlacek on the occasion of his 70th birthday.

Molecular geometries of 2,4,4,6-tetraphenyl-4*H*-pyran (*Ia*), 4,4-(biphenyl-2,2′-diyl)-2,6-diphenyl-4*H*-pyran (*Ib*) and their heterocyclic isomers *II–V* were optimized by the PM3 method and used for the calculation of electronic absorption spectra by the CNDO/S-CI procedure. Comparison of the theoretical data with experimental UV-VIS absorption spectra made possible to select hypervalent molecules *IIIa*, *IIIb*, *IVa* and *IVb* being responsible for the photocolouration of 4*H*-pyrans *Ia*, *Ib*, while compounds *Va*, *Vb*, *VI* and *VII* come into account as possible photodegradation products. The bleaching process of the UV illuminated compound *Ia* is analyzed in terms of dispersive first-order reaction kinetics.

Formation and properties of various hypervalent molecules belong to actual topics of current structural chemistry[1]. Besides the thermally generated unusual intermediates, some photochemically arising species have been reported. Thus, 2,4,4,6-tetraaryl-4*H*-thiopyrans have been observed to change their colours from white to green or violet by UV illumination due to a formation of some hypervalent photoisomers[2]. Similar species have been detected during the photocolouration of analogous 2,4,4,6-tetraaryl-1,4-dihydropyridines[3]. It may be expected that the tendence to form hypervalent states will be decreasing in the order of corresponding heteroatoms S >> NR > O. Although the photocolouration of 2,4,4,6-tetraaryl-4*H*-pyrans *I* has been repeatedly reported[4–6], the nature of corresponding coloured species has not yet been cleared up.

In this communication structures of the molecules *Ia–Va*, *Ib–Vb*, *VI* and *VII* are investigated using the quantum chemical PM3 and CNDO/S-CI methods and the results are compared with changes in experimental electronic absorption spectra of the 4*H*-pyrans *Ia* and *Ib* before and after their UV illuminations. In addition, the bleaching kinetic process of the illuminated compound *Ia* is studied.

EXPERIMENTAL

2,4,4,6-Tetraphenyl-4*H*-pyran (*Ia*), m.p. 187–188 °C, and 4,4-(biphenyl-2,2′-diyl)-2,6-diphenyl-4*H*-pyran (*Ib*), m.p. 171–173 °C, were prepared by employed procedures described previously[5,7]. UV-VIS absorption spectra were measured in solution using Hewlett–Packard 8451A recording spectrophotometer. The diffuse reflectance spectra of polycrystalline powders were recorded by a Perkin–Elmer–Hitachi 340 instrument under argon by the technique described in a previous paper[6].

CALCULATIONS

The molecular geometries of structures *Ia–Va*, *Ib–Vb*, *VI* and *VII* were obtained by the PM3 optimization[8] using the same parametrization as in previous communications[2,3]. Calculations of the electronic UV-VIS spectra were performed by the CNDO/S-CI method[9] using the parameters $\chi = 0.585$ for the integrals of π-bonds and the γ-sigma integrals were calculated by the usual procedure[10]. For all the studied MO models the size of CI was limited to 225 singly excited *i–j* configurations corresponding to electron transitions from the *i*-th occupied to the *j*-th unoccupied MO's.

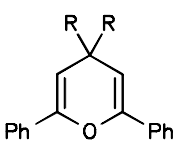

I

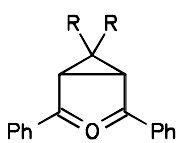

II

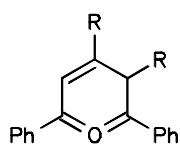

III

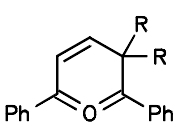

IV

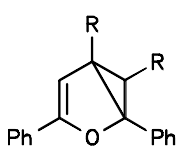

V

In formulae *I–V*:

a, R = Ph

b, R, R =

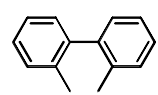

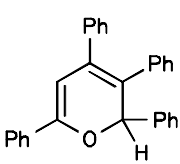

VI

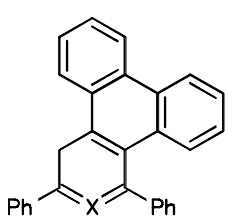

VII

a, X = O

b, X = S

c, X = NCH_3

RESULTS AND DISCUSSION

The adequacy of the PM3 and CNDO/S-CI methods to our purposes was tested by the comparison of the calculated and X-ray molecular geometries of 4*H*-pyran derivative *Ia* as well as of the experimental UV-absorption curves and theoretical electron transitions of both 4*H*-pyrans *Ia* and *Ib*. After that the calculations were extended to other isomeric molecules *IIa–Va*, *IIb–Vb*, *VI* and *VII*.

Molecular Energies and Structures

All PM3 models of molecules *Ia–VIIc* were successfully optimized. The calculated energy data are given in Table I. Expectably, the hypervalent molecules *II–IV* have been found to be rich of energy comparing to isomeric pyrans *I*, *VI* and 2,4-bridged isomers *V*. Since the energy stabilization of the hypervalent structures decreases in the order *III* > *IV* > *II* the molecules *IIIa*, *IIIb* may be considered as the first class candidates responsible for the photocolouration of 4*H*-pyrans *Ia* and *Ib*. Typical features of molecules *IIIa* and *IIIb* are shown in Figs 1 and 2. The molecular shapes are very similar to those of analogous hypervalent species in the thia-series[2].

The energy of phenathrenoid isomer *VIIa* was found to be less of 11.3 kcal mol^{-1} than that of the original hypervalent molecule *IIIb* (Table I). Hence, a possibility of the additional thermal isomerization *IIIb* → *VIIa* may be hardly excluded. Using the earlier reported energies[2,3] the same conlusions can be drawn for other heteroanalogues *VIIb*, *VIIc*.

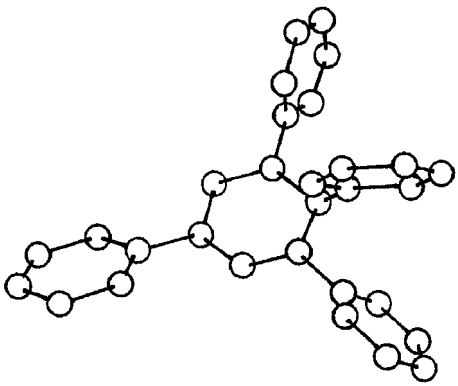

FIG. 1
Molecular skeleton of hypervalent species *IIIa* resulting from the PM3 optimization

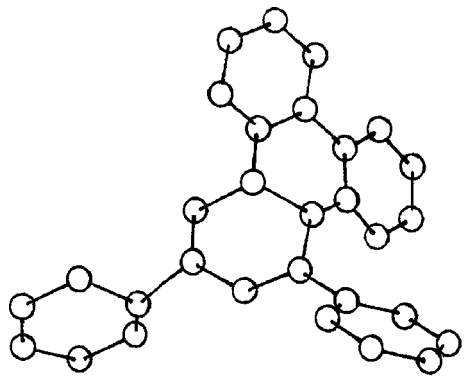

FIG. 2
Molecular skeleton of hypervalent species *IIIb* resulting from the PM3 optimization

Comparison of the PM3 calculated and X-ray[11] bond lengths and bond angles of 4*H*-pyran *Ia* (Table II) indicates a satisfactory agreement between the geometry characteristics. On the other hand, a worse agreement betweeen the PM3 calculated and X-ray

TABLE I
PM3 energies of molecules *I–VII*

Compound	ΔH_f[a]	E_{rel}[b]	Compound	ΔH_f[a]	E_{rel}[b]
Ia	107.04	0.0	*Ib*	122.87	0.0
IIa	148.71	41.67	*IIb*	156.52	33.65
IIIa	133.84	26.80	*IIIb*	134.25	11.38
IVa	140.70	33.66	*IVb*	142.38	19.51
Va	124.09	17.05	*Vb*	121.87	–1.00
VI	100.50	–6.54	*VIIa*	122.91	0.04
			VIIb	142.49	4.64
			VIIc	167.81	15.40

[a] Heats of formation in kcal mol^{-1}; [b] relative molecular energies in kcal mol^{-1} with respect to the parent heterocycles.

TABLE II
Comparison of calculated and observed bond lengths (Å), and bond angles (°) for 2,4,4,6-tetraphenyl-4*H*-pyran (*Ia*)

Bond	X-Ray[a]	PM3	Angle	X-Ray[a]	PM3
O1–C2	1.38	1.38	C6–O1–C2	118.5	116.7
C2–C3	1.32	1.34	O1–C2–C3	122.0	123.0
C3–C4	1.51	1.50	C2–C3–C4	124.5	123.0
C4–C5	1.51	1.51	C3–C4–C5	107.4	109.8
C5–C6	1.32	1.34	C4–C5–C6	124.3	122.5
C6–O1	1.38	1.38	Ph2–C2–O1	111.2	111.8
C2–Ph2	1.48	1.47	Ph4–C4–Ph4′	111.2	110.5
C4–P4	1.54	1.52	Ph4–C4–C5	107.3	111.7
C4–Ph4′	1.54	1.52	Ph4′–C4–C3	107.5	111.9
C6–Ph6	1.48	1.47	Ph6–C6–O1	110.9	111.8

[a] Taken from ref.[11].

dihedral angles does not enable to convincingly consider a final calculated molecular shape of *Ia* as an ideal one in solid state.

Charge Distribution

Some characteristics of the total and π-electron distributions for 4*H*-pyrans *Ia*, *Ib* and for probably their most stable hypervalent isomers *IIIa*, *IIIb* are given in Table III. Atomic net charges at the heterocyclic centres exhibit typical alternant charge distribution as in π-isoelectronic 1,4-dihydropyridines[3] which significantly differs from that of corresponding 4*H*-thiopyrans[2]. π-Electron distribution in the *III*-like hypervalent mole-

TABLE III
Calculated atomic net charges (. 10^3) and π-bond orders (. 10^3) for 4*H*-pyrans *Ia*, *Ib* and their hypervalent photoisomers *IIIa*, *IIIb*

Position	*Ia*	*Ib*	*IIIa*	*IIIb*	Bond	*Ia*	*Ib*	*IIIa*	*IIIb*
O1	–108	–123	+175	+165	O1–C2	97	91	418	397
C2	+85	+93	–131	–136	C2–C3	887	867	36	36
C3	–234	–223	+104	+100	C3–C4	31	37	33	32
C4	+172	+166	–139	–127	C4–C5	30	26	782	738
C5	–235	–210	–49	–57	C5–C6	887	907	198	214
C6	+86	+73	–189	–150	C6–O1	97	87	305	311

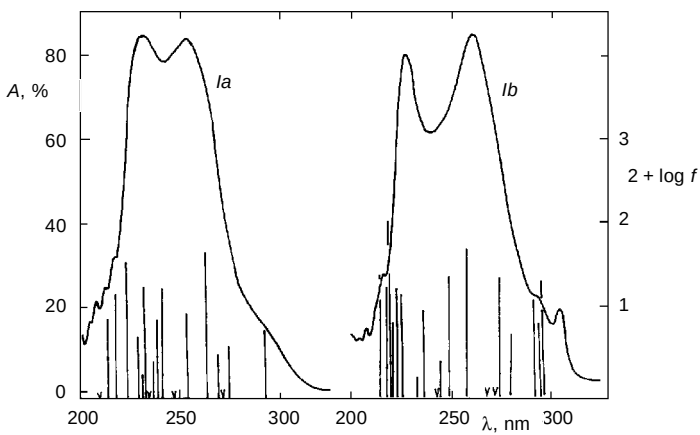

FIG. 3
Comparison of the absorption curves of 4*H*-pyrans *Ia* and *Ib* in acetonitrile with the CNDO/S-CI calculated spectra

cules are also of interest especially for the three-centre four-electron bonds C2–O1–C6 as well as for the two-centre two-electron double bonds C4–C5. Comparison of the corresponding π-bond orders for oxygen derivatives (Table III) with recently reported[2,3] data for corresponding aza and thia derivatives shows that the localization of the π-bonds in oxygen molecules *IIIa*, *IIIb* is only somewhat less developed than in appropriate aza and thia analogues (S > N > O for *IIIa* and N > S > O for *IIIb*, respectively). Hence, the generally discussed oxygen hypervalent structures[1] have been enriched by our novel examples.

Electronic Absorption Spectra

As follows from Fig. 3, the electronic absorption spectra of 4*H*-pyrans *Ia* and *Ib* can be satisfactory interpreted on the CNDO/S-CI level. The major diversity between the calculated π–π^* electron transitions of the both spectra consists in very different alignments and weights of the frontier $1 \rightarrow 1'$ excitations (Table IV).

Spectral characteristics calculated for the hypervalent photoisomers *II–IV* (Table IV) suggest that all these species should be coloured. However, comparison with the experimental spectral curves obtained after the UV illumination of 4*H*-pyrans *Ia* and *Ib* in the solid state (Figs 4 and 5) demonstrates that non-bridged hypervalent isomers *III* and *IV* should be responsible for the photocolouration. The fit of calculated visible absorption maxima for *IIIa*, *IIIb* (431.7, 567.7 nm and 448.3, 621.5 nm, respectively) with the absorption curve appears to be better than for *IVa*, *IVb* (451.8, 605.1 nm and 411.0,

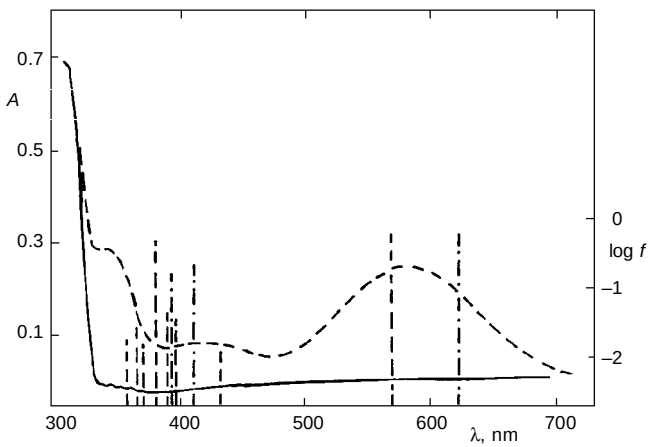

FIG. 4
Comparison of the absorption curves before (full line) and after (dashed line) UV illumination of 4*H*-pyran *Ia* (powder/MgO) with the CNDO/S-CI calculated spectra of hypervalent isomers *IIIa* (dashed lines) and *IVa* (dash-and-dot lines)

TABLE IV

Calculated electronic spectra of the studied compounds *I–VI* (wavelengths λ, nm; oscillator strengths *f*; assignments to electronic transitions *i–j* and weights *w*, %)

Compound	λ_{max}	*f*	*i–j*[a]	*w*	λ_{max}	*f*	*i–j*[a]	*w*
Ia	294.9	0.0544	1–1′	86.8	237.2	0.0273	1–9′	26.2
	275.8	0.0058	1–4′	19.8	235.2	0.0044	1–3′	66.7
	274.8	0.0218	3–5′	22.0	234.0	0.2214	3–1′	52.3
	272.9	0.0005	3–7′	18.0	233.2	0.0233	1–7′	60.2
	270.5	0.0165	1–3′	14.0	230.1	0.0431	1–4′	46.4
	264.5	0.4468	1–2′	76.4	222.0	0.3087	1–10′	23.9
	254.1	0.0533	1–6′	64.5	219.0	0.1667	2–2′	25.2
	247.7	0.0014	1–8′	64.3	214.2	0.0182	3–7′	21.1
	241.7	0.2140	2–1′	44.4	214.0	0.0419	3–6′	17.7
	239.8	0.0466	1–5′	23.7	211.0	0.0073	2–6′	31.4
Ib	296.9	0.2268	2–1′	22.5	246.0	0.0022	1–7′	47.8
	295.4	0.0546	2–6′	21.5	237.3	0.0947	1–8′	43.2
	292.2	0.1086	1–2′	51.2	232.2	0.0142	1–4′	44.9
	276.9	0.0516	2–1′	26.6	226.1	0.1298	3–2′	52.8
	274.2	0.2507	1–1′	21.7	224.2	0.1587	3–3′	23.5
	272.1	0.0062	1–5′	37.8	222.4	0.0528	1–5′	19.1
	268.8	0.0074	5–4′	36.0	221.6	0.1812	1–5′	26.4
	257.0	0.4778	1–3′	44.2	220.7	0.8521	4–1′	22.0
	249.7	0.2340	2–2′	28.8	218.0	0.1290	4–2′	31.3
	246.7	0.0242	1–6′	41.9	215.6	0.1922	1–10′	21.4
IIa	505.2	1.0276	1–1′	96.8	344.2	0.0675	1–5′	41.6
	367.9	0.0015	1–2′	86.5	331.4	0.0531	1–8′	49.6
	358.0	0.0141	1–4′	76.5	313.6	0.0038	1–7′	46.6
	354.4	0.0208	1–6′	87.6	312.4	0.0020	1–3′	42.7
IIb	500.4	1.2048	1–1′	97.6	340.7	0.0759	1–3′	67.2
	385.2	0.1186	1–2′	80.3	319.0	0.0635	1–5′	51.9
	348.8	0.0188	1–6′	87.4	304.6	0.0020	1–7′	45.0
	348.4	0.0233	1–4′	86.9	288.1	0.0026	1–9	80.8
IIIa	567.7	0.3413	1–1′	94.3	368.7	0.0158	1–7′	78.7
	431.7	0.0104	1–3′	86.4	363.2	0.0601	1–4′	31.3
	393.8	0.0396	1–2′	72.6	357.1	0.0182	1–8′	89.5
	389.3	0.0436	1–5′	31.4	346.0	0.0016	1–6′	65.4
	379.7	0.3336	1–9′	56.8	296.0	0.0064	1–10′	69.6
IIIb	621.5	0.2875	1–1′	92.6	370.7	0.0168	1–6′	69.3
	448.3	0.2851	1–2′	81.8	349.9	0.0139	1–7′	93.0
	398.9	0.0234	1–4′	68.9	326.6	0.0407	1–8′	66.0
	384.2	0.1452	1–3′	49.2	326.0	0.0508	2–1′	57.4
	378.3	0.1224	1–5′	40.5	301.9	0.0398	1–9′	67.1

TABLE IV
(*Continued*)

Compound	λ_{max}	*f*	*i–j*[a]	*w*	λ_{max}	*f*	*i–j*[a]	*w*
IVa	623.1	0.3451	1–1′	95.3	358.3	0.1038	1–7′	67.2
	411.0	0.2536	1–2′	53.8	349.0	0.0113	1–6′	60.4
	392.8	0.1660	1–5′	58.2	348.5	0.0181	1–8′	66.9
	379.9	0.0251	1–3′	60.9	343.9	0.1480	1–9′	77.7
	370.1	0.1110	1–4′	39.9	299.3	0.1741	2–1′	82.0
IVb	605.1	0.4028	1–1′	96.1	364.0	0.2006	1–6′	68.3
	451.8	0.0083	1–2′	84.8	351.4	0.0432	1–8′	55.8
	393.7	0.2497	1–4′	78.2	350.1	0.0173	1–7′	81.0
	379.5	0.0170	1–3′	87.0	312.0	0.1302	2–1′	71.7
	367.8	0.0178	1–5′	70.8	295.3	0.0132	1–9′	95.6
Va	285.2	0.5864	1–1′	67.7	271.8	0.0070	3–3′	19.5
	282.7	0.2419	1–5′	30.4	268.2	0.0027	4–2′	24.9
	275.9	0.0108	1–8′	13.6	241.3	0.0117	1–6′	54.1
Vb	299.4	0.1556	1–1′	22.0	283.0	0.2231	1–6′	26.6
	296.7	0.0984	2–1′	26.3	279.4	0.2196	2–7′	25.7
	285.4	0.5592	1–2′	44.4	266.5	0.0030	7–4′	25.5
VI	309.6	0.3778	1–1′	89.5	272.6	0.0243	1–4′	13.5
	284.0	0.0027	1–3′	26.0	271.8	0.0028	1–3′	41.5
	277.8	0.0196	1–7′	18.4	269.5	0.0084	4–5′	12.4

[a] Excitation from the *i*-th occupied MO to the *j*-th unoccupied MO.

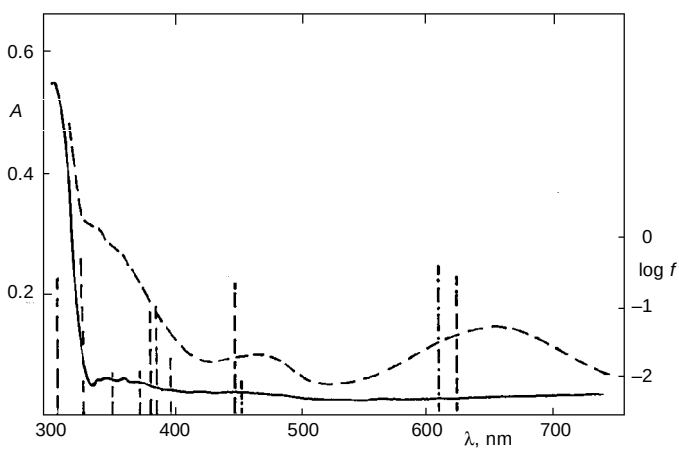

FIG. 5
Comparison of the absorption curves before (full line) and after (dashed line) UV illumination of 4*H*-pyran *Ib* (powder/MgO) with the CNDO/S-CI calculated spectra of hypervalent isomers *IIIb* (dashed lines) and *IVb* dash-and-dot lines)

623.1 nm, respectively) although no definitive discrimination between them is possible. A correctly predicted red shift of the long-wavelength absorption maximum due to the 2,2′-linked substructure of the 4,4-aryl groups in UV illuminated pyran *Ib* ("bridged effect", see refs[2,3]) may be regarded as an additional support for relevance of the alternatives *IIIa*, *IIIb*. The predicted visible absorption for the 3,5-bridged photoisomers *IIa*, *IIb* (505.2 and 500.4 pm) seems to be too short-wavelength.

In connection with the mentioned "bridged effect" a possibility of an additional thermal isomerization *IIIb* → *VIIa* was investigated. From data given in Table V it follows that the predicted visible absorption of *VIIa*, i.e. 405.8, 438.5 and 591.8 nm, does not improve fit of the calculation with the experimental absorption curve in Fig. 5. The same conclusions can be drawn on the basis of comparison of other data in Table V (structures *VIIb*, *VIIc*) with the previously reported[2,3] absorption curves. Hence, no *VII*-like structures have to be considered for the photocolouration phenomena. Additional data in Table IV show that 2,4-bridged isomers *Va*, *Vb* as well as 2*H*-pyran *VI* will not be couloured substances. Nevertheless, the presence of them might be hardly excluded in mixtures of photodegradation products from 4*H*-pyrans *Ia*, *Ib*.

Kinetics of the Bleaching Process

The thermal course of bleaching of solid 4*H*-pyran *Ia* at different temperatures is given in Fig. 6*a*. The curves show the normalized concentration $[M(t)/[M(0)]$ of the coloured species vs time (t), calculated using the Munk–Kubelka function[12]. A multiexponential analysis of the bleaching kinetics gave good two-exponential fit – see Eq. (*1*)

$$[M(t)] = [M(0)] \{A_1 \exp(-t/\tau_1) + A_2 \exp(-t/\tau_2)\} . \qquad (1)$$

TABLE V
Calculated visible electronic absorptions of hypervalent heteroanalogues *VII* (wavelengths λ, nm; oscillator strengths *f*; assignments to electronic transitions *i*–*j* and weights *w*, %)

Compound	λ_{max}	*f*	*i*–*j*[a]	*w*	λ_{max}	*f*	*i*–*j*[a]	*w*
VIIa	591.8	0.6939	1–1′	93.9	405.8	0.0615	1–2′	68.7
	438.5	0.2527	1–3′	71.9	362.8	0.0063	1–5′	88.1
VIIb	606.6	0.7941	1–1′	89.9	411.5	0.0343	1–3′	81.4
	475.6	0.1551	1–2′	64.1	383.8	0.5567	2–1′	69.6
VIIc	573.6	0.3577	1–1′	96.0	414.9	0.0096	1–4′	90.6
	422.9	0.0982	1–2′	85.3	390.8	0.1151	1–5′	41.0

[a] Excitation from the *i*-th occupied MO to the *j*-th unoccupied MO.

The obtained parameters are given in Table VI. Although the two-exponential fit offered very good results, the use of the statistical distribution of thermodynamic reaction parameters was tested too. The optical properties of disordered polycrystalline materials must be regarded as resulting from a set of individual processes of different rates, weighted by the distribution of parameters. If the kinetics are first-order at each site, the superposition of time-independent rates will cause the overall rate of the process to be time dependent. The corresponding decay law for these dispersive processes[13] differs from the pure exponential form and follows exp $(-t^{\alpha})$, where t is the time and α is the dispersion parameter which measures the strength of dispersion. Hence, the photochromic bleaching process of *Ia* could be described by a stretched exponential equation (*2*) (refs[14,15])

$$[M(t)] = [M(0)] \exp -(\nu t)^{\alpha} , \qquad (2)$$

where $0 < \alpha < 1$ measures the deviation from the pure exponential behaviour and ν is the decay rate constant.

Decay kinetics given in Fig. 6*a* were fitted by stretched exponential according to Eq. (*2*). Linearity of the ln $\{[M(t)]/[M(0)]\}$ vs t^{α} curves given in Fig. 6*b* documents the dispersive nature of the bleaching process. The best fits were obtained with the following parameters: T = 284, 303, 316, 322 and 339 K; α = 0.733, 0.805, 0.947, 0.961 and 0.991.

In irregular systems, such as our polycrystalline materials are, the activation energies and entropies of the photochromic back reaction depend on the local geometry around the reaction species *IIIa* (*IVa*) and consequently are quantities with statistical variation.

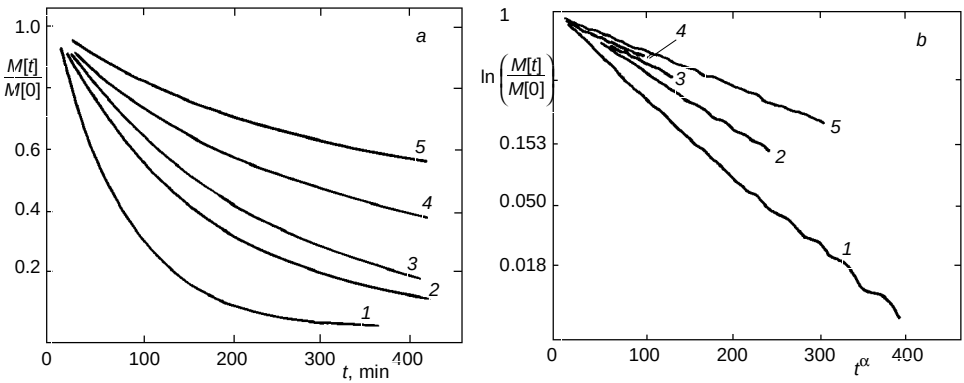

FIG. 6

Decolouration kinetics of polycrystalline 2,4,4,6-tetraphenyl-4*H*-pyran (*Ia*) at different temperatures: *1* 339 K, *2* 322 K, *3* 316 K, *4* 303 K, *5* 284 K; *a*, *b* see text

The thermally induced decolourating reaction, probably *IIIa* → *Va*, is associated with the rate constant ν(*E*) according to Eq. (*3*),

$$\nu(E) = \nu_0 \exp\left[-(E_m - E)/kT\right] , \qquad (3)$$

TABLE VI
Parameters τ_1 and τ_2 from Eq. (*1*)

T, K	τ_1, min	τ_2, min
284	553	3 350
303	339	1 120
316	231	271
322	171	208
339	77.3	94.4

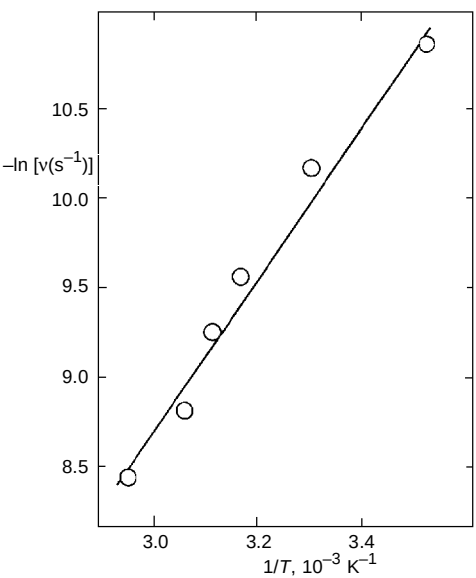

FIG. 7
Dependence of the frequency factor on the reciprocal temperature for polycrystalline 2,4,4,6-tetraphenyl-4*H*-pyran (*Ia*)

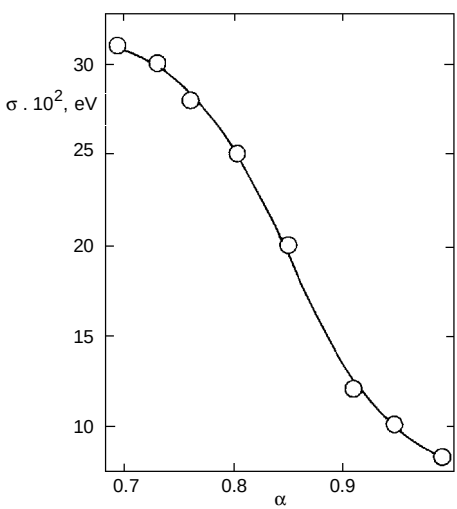

FIG. 8
Dependence of the energetical bandwidth σ on the dispersion parameter α for polycrystalline 2,4,4,6-tetraphenyl-4*H*-pyran (*Ia*)

where ν_0 is the frequency factor. Since the energy difference between the gound state (E) and the maximum of the energy barrier (E_m) depends on a set of conformational parameters, each varying statistically, the most probable distribution function for ($E_m - E$) was assumed[15] to be a Gaussian one characterized by its width σ. Therefore, the time dependence of the concentration of *IIIa* (*IVa*) should be the convolution of first-order decay functions reflecting the unimolecular nature of the process and the distribution function for the reaction rates defined[14] by Eq. (*4*).

$$[M(t)] = \{[M(0)]/(2\pi\sigma^2)\} \int \exp[-(E_0 - E)^2/2\sigma^2] \exp[-\nu(E)t]\mathrm{d}E \qquad (4)$$

The experimental results, given in Fig. 6*a*, were fitted using Eq. (*4*). The best fits for temperatures T = 284, 303, 316, 322 and 339 K were obtained with the following parameters: σ = 0.030, 0.025, 0.011, 0.012 and 0.010 eV; $\nu = 1.94 \cdot 10^{-5}$, $3.84 \cdot 10^{-5}$, $7.07 \cdot 10^{-5}$, $9.60 \cdot 10^{-5}$ and $2.18 \cdot 10^{-4}$ s^{-1}.

The Gaussian widths of the distributions o. the activation energies decreased with temperature. The activation energy ($E_m - E$) = (0.37 ± 0.02) eV and the average frequency factor ν_0 = (55 ± 3) s^{-1} were obtained from the dependence of the fitted parameters ν on the reciprocal temperatures given in Fig. 7. Thus, with respect to the temperature range 284 K < T < 339 K, the experimental data can be interpreted in terms of a single temperature-activated rate process, the only temperature-dependent quantity being the fluctuation of the activation energies. Figure 8 shows a correlation between the dispersion parameter α (obtained from the experimental $[M(t)]/[M(0)]$ vs t^{α} curves, see Eq. (*1*), and the fluctuation σ of the activation energy derived from the calculated $[M(t)]$ curves according to Eq. (*3*).

CONCLUSIONS

The photocolouration of the both 4*H*-pyrans *Ia*, *Ib* has been fully described by irreversible formation of hypervalent photoisomers *IIIa*, *IIIb* and partly *IVa*, *IVb*. Thus, the π-methane rearrangements of the starting heterocycles may be considered as leading processes of the optical changes. From this point of view, the behaviour of the studied compounds *Ia*, *Ib* resembles to a large extent the photocolouration of corresponding aza and thia analogues[2,3].

This work was supported by a grant from the University Development Foundation No. 0180/7/95 issued by Ministry of Education of the Czech Republic.

REFERENCES

1. Ramsden C. A.: Chem. Soc. Rev. *23*, 111 (1994); and references therein.
2. Bohm S., Sebek P., Nespurek S., Kuthan J.: Collect. Czech. Chem. Commun. *59*, 1115 (1994).
3. Bohm S., Hocek M., Nespurek S., Kuthan J.: Collect. Czech. Chem. Commun. *59*, 262 (1994).

4. Peres de Carvalho A.: Ann. Chim. (Paris) *4*, 449 (1935).
5. Kurfurst A., Zeleny J., Schwarz M., Kuthan J.: Chem. Papers *41*, 623 (1987).
6. Nespurek S., Schwarz M., Bohm S., Kuthan J.: J. Photochem. Photobiol., A *60*, 345 (1991).
7. Sebek P., Nespurek S., Hrabal R., Adamec M., Kuthan J.: J. Chem. Soc., Perkin Trans. 2 *1992*, 1301.
8. Stewart J. J. P.: J. Comput. Chem. *10*, 209, 221 (1989).
9. Del Bene J., Jaffe H. H.: J. Chem. Phys. *48*, 1807, 4050 (1968).
10. Mataga N., Nishimoto E.: Z. Phys. Chem. *13*, 140 (1957).
11. Vojtechovsky J., Hasek J.: Acta Crystallogr., C *46*, 1727 (1990).
12. Kortum G.: *Reflexionspektroskopie*, p. 111. Springer, Berlin 1969.
13. Richert R.: Chem. Phys. Lett. *118*, 534 (1985).
14. Kohlrausch R.: Ann. Phys. (Leipzig) *12*, 393 (1847).
15. Richert R., Bassler H.: Chem. Phys. Lett. *116*, 302 (1985).